

2. R. A. Diehl, *The Olmecs: America's First Civilization* (Thames & Hudson, London, 2005).
3. M. E. D. Pohl, K. O. Pope, C. von Nagy, *Science* **298**, 1984 (2002).
4. V. Scheil, *Documents en Écriture Proto-Élamites* (Ernest Leroux, Paris, 1905).
5. J. Marshall, *Illus. Lond. News* **20**, 528 (1924).
6. H. Holmes, *Am. Anthropol.* **9**, 691 (1907).
7. P. Ortiz, C. Rodriguez, *Arqueología*, in press.
8. M. D. Coe, R. A. Diehl, *In the Land of the Olmec* (Univ. of Texas Press, Austin, TX, 1980).
9. S. Houston, in *The First Writing*, S. Houston, Ed. (Cambridge Univ. Press, Cambridge, 2004), p. 284.
10. M. D. Coe, *Breaking the Maya Code* (Thames & Hudson, London, rev. ed., 1999), p. 13.
11. S. D. Houston, M. D. Coe, *Mexicon* **25**, 151 (2004).
12. K. A. Taube, *Olmec Art at Dumbarton Oaks* (Dumbarton Oaks, Washington, DC, 2004).
13. K. A. Taube, in *The Olmec World: Ritual and Rulership*, J. Guthrie (Princeton Univ. Art Museum, Princeton, NJ, 1995).
14. T. D. Sullivan, *A Scattering of Jades: Stories, Poems, and Prayers of the Aztecs* (Univ. of Arizona Press, Tucson, AZ, 1994), pp. 229 and 258.
15. K. A. Taube, *Olmec Art at Dumbarton Oaks* (Dumbarton Oaks, Washington, DC, 2004).
16. D. Cheetham, J. E. Clark, in *XIX Simposio de Investigaciones Arqueológicas en Guatemala, 2005*, J. P. Laporte, B. Arroyo, H. E. Mejía, Eds. (Ministerio de Cultura y Deportes, Guatemala City, Guatemala, 2006).
17. P. D. Joralemon, *A Study of Olmec Iconography* (Dumbarton Oaks, Washington, DC, 1971).
18. P. Ortiz, C. Rodriguez, in *Olmec Art and Archaeology in Mesoamerica*, J. E. Clark, M. E. Pye, Eds. (Yale Univ. Press, New Haven, CT, 2000), pp. 75–93.
19. K. H. Basso, N. Anderson, *A Western Apache Writing System* (Peter de Ridder, Lisse, Netherlands, 1975), p. 5.
20. S. D. Houston, J. Baines, J. Cooper, *Comp. Stud. Soc. Hist.* **45**, 430 (2003).
21. Access to the Cascajal block was facilitated by members of the Patronato Prodefensa del Patrimonio Cultural Lomas de Tacamichapa, Cástulo Gabriel Cruz, President. The Centro Regional, Veracruz, of the INAH made the visit possible. J. Clark and D. Cheetham commented on the manuscript, as did several anonymous reviewers. Z. Nelson helped prepare figures.

Supporting Online Material

www.sciencemag.org/cgi/content/full/313/5793/1610/DC1
Materials and Methods
Figs. S1 to S3

19 June 2006; accepted 8 August 2006
10.1126/science.1131492

REPORTS

Probing Nanoscale Ferroelectricity by Ultraviolet Raman Spectroscopy

D. A. Tenne,^{1*} A. Bruchhausen,² N. D. Lanzillotti-Kimura,² A. Fainstein,² R. S. Katiyar,³ A. Cantarero,⁴ A. Soukiassian,⁵ V. Vaithyanathan,⁵ J. H. Haeni,⁵ W. Tian,⁵ D. G. Schlom,⁵ K. J. Choi,⁶ D. M. Kim,⁶ C. B. Eom,⁶ H. P. Sun,⁷ X. Q. Pan,⁷ Y. L. Li,^{5,8} L. Q. Chen,⁵ Q. X. Jia,⁸ S. M. Nakhmanson,⁹ K. M. Rabe,⁹ X. X. Xi^{1,5}

We demonstrated that ultraviolet Raman spectroscopy is an effective technique to measure the transition temperature (T_c) in ferroelectric ultrathin films and superlattices. We showed that one-unit-cell-thick BaTiO₃ layers in BaTiO₃/SrTiO₃ superlattices are not only ferroelectric (with T_c as high as 250 kelvin) but also polarize the quantum paraelectric SrTiO₃ layers adjacent to them. T_c was tuned by ~500 kelvin by varying the thicknesses of the BaTiO₃ and SrTiO₃ layers, revealing the essential roles of electrical and mechanical boundary conditions for nanoscale ferroelectricity.

Ferroelectricity at the nanoscale has emerged as fertile ground for new physical phenomena and devices (1–3). Shrinking dimensions demand characterization techniques that are capable of probing the properties of ferroelectrics in, for example, ultrathin films and superlattices. In particular, it is difficult to measure the ferroelectric phase transition tempera-

ture T_c in such systems, and the T_c information is largely missing in reports of ferroelectricity in nanoscale ultrathin films and superlattices (4, 5). One fundamental property of ferroelectrics that changes qualitatively during the phase transition is the dynamics of lattice vibrations (6). Thus, its temperature dependence allows the determination of T_c . Although lattice dynamics in ferroelectric films (7, 8) and superlattices (9) from 150 nm to 2 μ m in thickness have been investigated previously, such studies are very difficult on films thinner than ~100 nm. We report the use of ultraviolet (UV) Raman spectroscopy on BaTiO₃/SrTiO₃ superlattices with total thicknesses down to 24 nm, which enabled us to measure the T_c of the BaTiO₃ layers in the superlattices. We found that the BaTiO₃ layers are ferroelectric even when their thickness is only one unit cell (0.4 nm) and that they can induce polarization in the adjacent paraelectric SrTiO₃ layers that are much thicker. By varying the thickness of both the BaTiO₃ and SrTiO₃ layers, T_c was tuned from 250 K below to 235 K above the bulk value of BaTiO₃ (403 K). This result shows that under favorable electrical and mechanical boundary conditions, ferroelectricity is robust in nanoscale systems.

Conventional visible Raman spectroscopy works poorly for thin films of ferroelectrics and other wide-band-gap materials because the visible photon energy is much smaller than the band gap (10). Consequently, the absorption is extremely weak and the penetration depth is large, allowing light to travel through the film into the substrate, which generates overwhelming signals in the Raman spectra. For UV excitation, the photon energy is above the band gaps of ferroelectrics, leading to a much stronger absorption and a shorter penetration depth, preventing light from entering the substrate. UV excitation near the band gap also leads to strong resonance enhancement of Raman signals. This is demonstrated by Fig. 1, where Raman spectra of a BaTiO₃/SrTiO₃ superlattice

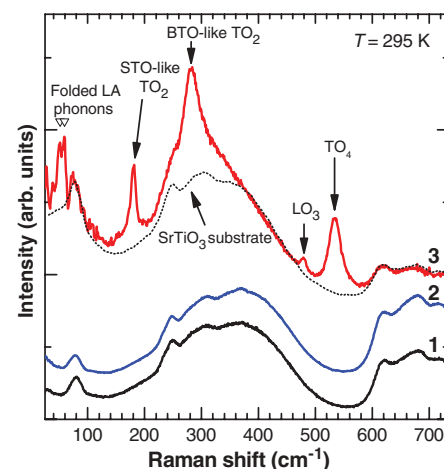


Fig. 1. Room-temperature Raman spectra of (1) a bare SrTiO₃ substrate (black curve); (2) a (BTO₃/STO₄) × 25 superlattice ($T_c = 530$ K, blue curve) measured with visible excitation (514.5 nm); and (3) the same superlattice measured with 351.1-nm UV excitation (red curve). The dashed black line shows the bare SrTiO₃ substrate spectrum measured with 351.1-nm UV excitation. Triangles show the calculated frequencies of the first folded LA doublet. arb., arbitrary.

¹Department of Physics, The Pennsylvania State University, University Park, PA 16802, USA. ²Centro Atómico Bariloche y Instituto Balseiro, Comisión Nacional de Energía Atómica, 8400 San Carlos de Bariloche, Argentina. ³Department of Physics, University of Puerto Rico, San Juan, Puerto Rico 00931–3343, USA. ⁴Materials Science Institute, University of Valencia, Post Office Box 22085, E-46071 Valencia, Spain. ⁵Department of Materials Science and Engineering, The Pennsylvania State University, University Park, PA 16802, USA. ⁶Department of Materials Science and Engineering, University of Wisconsin, Madison, WI 53706, USA. ⁷Department of Materials Science and Engineering, University of Michigan, Ann Arbor, MI 48109, USA. ⁸Materials Science and Technology Division, Los Alamos National Laboratory, Los Alamos, NM 87545, USA. ⁹Department of Physics and Astronomy, Rutgers, The State University of New Jersey, 136 Frelinghuysen Road, Piscataway, NJ 08854–8019, USA.

*To whom correspondence should be addressed: Department of Physics, Boise State University, 1910 University Drive, Boise, ID 83725–1570, USA. E-mail: dmitritenne@boisestate.edu

Report Documentation Page

*Form Approved
OMB No. 0704-0188*

Public reporting burden for the collection of information is estimated to average 1 hour per response, including the time for reviewing instructions, searching existing data sources, gathering and maintaining the data needed, and completing and reviewing the collection of information. Send comments regarding this burden estimate or any other aspect of this collection of information, including suggestions for reducing this burden, to Washington Headquarters Services, Directorate for Information Operations and Reports, 1215 Jefferson Davis Highway, Suite 1204, Arlington VA 22202-4302. Respondents should be aware that notwithstanding any other provision of law, no person shall be subject to a penalty for failing to comply with a collection of information if it does not display a currently valid OMB control number.

1. REPORT DATE 15 SEP 2006	2. REPORT TYPE	3. DATES COVERED 00-00-2006 to 00-00-2006			
4. TITLE AND SUBTITLE Probing Nanoscale Ferroelectricity by Ultraviolet Raman Spectroscopy		5a. CONTRACT NUMBER			
		5b. GRANT NUMBER			
		5c. PROGRAM ELEMENT NUMBER			
6. AUTHOR(S)		5d. PROJECT NUMBER			
		5e. TASK NUMBER			
		5f. WORK UNIT NUMBER			
7. PERFORMING ORGANIZATION NAME(S) AND ADDRESS(ES) University of Wisconsin-Madison, Department of Materials Science and Engineering, Madison, WI, 53706		8. PERFORMING ORGANIZATION REPORT NUMBER			
9. SPONSORING/MONITORING AGENCY NAME(S) AND ADDRESS(ES)		10. SPONSOR/MONITOR'S ACRONYM(S)			
		11. SPONSOR/MONITOR'S REPORT NUMBER(S)			
12. DISTRIBUTION/AVAILABILITY STATEMENT Approved for public release; distribution unlimited					
13. SUPPLEMENTARY NOTES					
14. ABSTRACT					
15. SUBJECT TERMS					
16. SECURITY CLASSIFICATION OF:			17. LIMITATION OF ABSTRACT Same as Report (SAR)	18. NUMBER OF PAGES 3	19a. NAME OF RESPONSIBLE PERSON
a. REPORT unclassified	b. ABSTRACT unclassified	c. THIS PAGE unclassified			

measured with visible (514.5 nm) and UV (351.1 nm) excitations are shown. The substrate features dominate the 514.5-nm spectrum, but they are greatly reduced in the UV spectrum, in which peaks of superlattice phonons are clearly observed.

UV Raman spectroscopy has not been widely used for measurements of ferroelectric films because of technical difficulties such as lower throughput efficiency, insufficient dispersion, and higher stray light level of UV Raman spectrometers as compared to those operating in the visible range. Recently, room-temperature measurement of SrTiO₃ films using 325-nm excitation has been reported (11). The recent progress in UV Raman instrumentation has made the measurement of ferroelectric films possible. In our experiment, a triple monochromator was used to provide high resolution and effective reduction of stray light (12). Powerful laser sources and optimized optical paths were used to improve the throughput. With these setups, we have measured Raman scattering in BaTiO₃/SrTiO₃ superlattices as thin as 24 nm and in (Ba_{0.5}Sr_{0.5})TiO₃ films that were 10 nm thick.

The BaTiO₃/SrTiO₃ superlattices are denoted by (BTO_{*n*}/STO_{*m*}) × number of periods, where *n* and *m* refer to the thickness, in unit cells, of the BaTiO₃ and SrTiO₃ layers, respectively. They were all grown on (001) SrTiO₃ substrates. Details of the sample preparation by reactive molecular-beam epitaxy (13) and structural characterization are presented in the supporting online material (12).

Curve 3 in Fig. 1 is typical of the UV Raman spectra of BaTiO₃/SrTiO₃ superlattices below *T_c*, exhibiting strong first-order (single-phonon) peaks as labeled in the figure. Weak second-order (two-phonon) features from the SrTiO₃ substrate can be seen between 600 and 700 cm⁻¹ and as a background in the range from 200 to 500 cm⁻¹. The phonon mode assignment was made by comparison with the spectra of SrTiO₃ and BaTiO₃ single crystals (12) and with the help of first-principles calculations. The lines at about 290 cm⁻¹ have similar positions and shapes to the TO₂ modes of A₁ symmetry of the tetragonal-phase BaTiO₃ (14, 15); thus, they are assigned to the BaTiO₃ layers. The line at about 180 cm⁻¹ corresponds closely to the TO₂ line in the electric field-induced Raman spectrum of SrTiO₃ crystals (16). It is not from the SrTiO₃ substrate, because the first-order Raman lines are symmetry-forbidden in bulk SrTiO₃ (17). Although the TO₁ mode of A₁ symmetry of BaTiO₃ is at about the same position (177 cm⁻¹), it has markedly different relative intensity and shape (14) from the 180-cm⁻¹ line. Therefore, we attribute this line to the TO₂ phonon in the SrTiO₃ layers. The LO₃ and TO₄ modes involve both SrTiO₃ and BaTiO₃ layers and extend through the superlattice. A doublet of folded longitudinal acoustic (LA) phonons due to the superlattice periodicity (18) is also observed. The two triangles indicate the pre-

dicted first-doublet frequencies by an elastic continuum model (19). The observation of the LA phonon folding suggests that these superlattices possess the requisite structural quality for acoustic Bragg mirrors and cavities used for coherent phonon generation (20, 21).

Bulk crystalline BaTiO₃ is cubic and paraelectric above *T_c* = 403 K, becomes tetragonal and ferroelectric below *T_c*, and goes through additional transitions to orthorhombic at 278 K and rhombohedral at 183 K (22). Bulk crystalline SrTiO₃ is paraelectric at all temperatures

because of quantum fluctuations (23). The temperature evolution of Raman spectra for two superlattice samples is shown in Fig. 2A (BTO₂/STO₁₃) × 20 and Fig. 2B (BTO₈/STO₄) × 10. The shapes and positions of the BaTiO₃ lines at low temperatures are characteristic of BaTiO₃ in the tetragonal phase (12, 14, 15), indicating that the BaTiO₃ layers are tetragonal and ferroelectric below *T_c*. The presence of the first-order Raman lines of SrTiO₃ shows that the SrTiO₃ layers are polar because the first-order lines are symmetry-forbidden in nonpolar

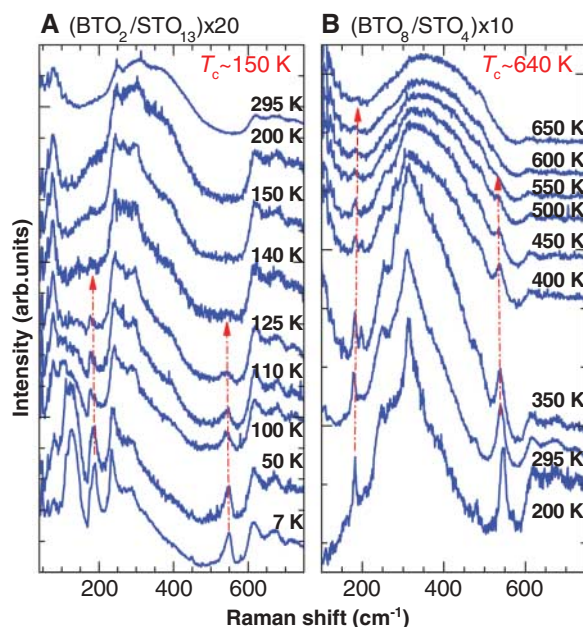


Fig. 2. Temperature evolution of UV Raman spectra of superlattices (BTO₂/STO₁₃) × 20 (A) and (BTO₈/STO₄) × 10 (B). The red arrows mark the SrTiO₃-like TO₂ mode at 180 cm⁻¹ and the TO₄ mode at about 530 cm⁻¹, whose intensities decrease as the temperature increases and disappear at *T_c*.

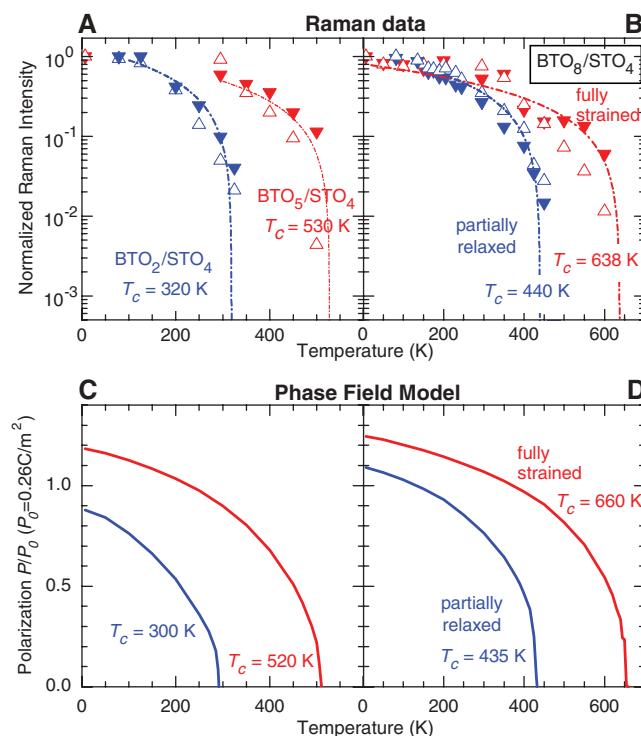


Fig. 3. Temperature dependencies of normalized Raman intensities of TO₂ (solid triangles) and TO₄ (open triangles) phonons for (BTO₂/STO₄) × 40 and (BTO₂/STO₄) × 25 (A) and (BTO₈/STO₄) × 10 and (BTO₈/STO₄) × 40 (B). Sample (BTO₈/STO₄) × 40 is partially relaxed, whereas the other three samples are commensurate with the SrTiO₃ substrate. The dash-dotted lines are fits to a linear temperature dependence. (C and D) The 3D phase-field model calculations of polarization as a function of temperature in the same superlattice samples. Polarization (*P*) is given as a fraction of the polarization of bulk BaTiO₃ (*P₀* = 0.26 C/m²).

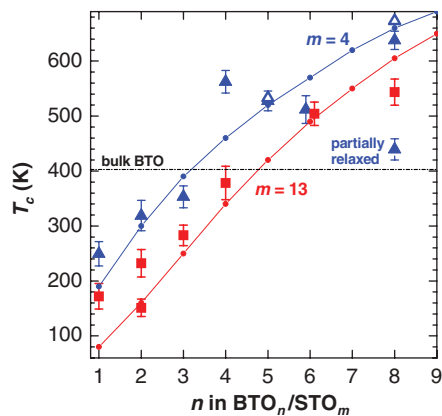


Fig. 4. Dependence of T_c on n and m in superlattices $\text{BTO}_n/\text{STO}_m$. Blue symbols are for $m = 4$ and red symbols are for $m = 13$. Open triangles are from temperature-dependent XRD measurements. Circles with lines are from the 3D phase-field model calculations. The black horizontal dash-dotted line shows the T_c in bulk BaTiO_3 .

SrTiO_3 (17). The intensities of the first-order superlattice phonons decrease as the temperature increases and disappear at T_c . Above T_c , the spectra contain only the second-order features, as expected from the symmetry selection rules. When the BaTiO_3 layers are paraelectric, the induced polarization in the SrTiO_3 layers also disappears.

By plotting the first-order Raman intensity as a function of temperature, we can accurately determine T_c as the temperature where the intensity becomes zero. For this purpose, the TO_2 and TO_4 phonon lines are the most suitable because they do not overlap with the second-order features. The results, with the phonon intensities normalized by the Bose factor $n + 1 = \{1 - \exp[-(\hbar/2\pi)\omega/kT]\}^{-1}$ (where \hbar is Planck's constant, ω is phonon frequency, k is Boltzmann's constant, and T is temperature) and by the intensities at 7 K, are presented for four superlattices: $(\text{BTO}_2/\text{STO}_4) \times 40$ and $(\text{BTO}_5/\text{STO}_4) \times 25$ in Fig. 3A and $(\text{BTO}_8/\text{STO}_4) \times 10$ and $(\text{BTO}_8/\text{STO}_4) \times 40$ (strain partially relaxed) in Fig. 3B. Both TO_2 and TO_4 phonons show similar behaviors, and the dashed-dotted lines are linear fits to the average of the two modes. The linear fit corresponds to a parabolic decrease of polarization with temperature, because Raman intensity is proportional to the square of atomic displacement. The intersection of a dash-dotted line with the horizontal axis is taken as the T_c of the sample.

The temperature dependence of polarization from a phase-field model calculation (24) is plotted in Fig. 3, C and D, for the same samples as in Fig. 3, A and B. The model assumes that the BaTiO_3 and SrTiO_3 layers in the superlattices have their respective bulk elastic and thermodynamic properties. The in-plane lattice constant is commensurately constrained to

the SrTiO_3 substrate except for the partially relaxed case, and the top surface is stress-free. The surface depolarization field is ignored and a short-circuit electrostatic boundary condition is employed. A computational cell of 64 nm along the two in-plane directions and one unit cell along the growth direction was employed. The corresponding three-dimensional (3D) time-dependent Ginzburg-Landau equations are then numerically solved using the perturbation method with semi-implicit Fourier-spectral algorithms (25). The result reveals a spontaneous polarization along the growth direction with multiple 180° domains in the BaTiO_3 layers, which induces polarization in the adjacent SrTiO_3 layers, whose magnitude and distribution vary with the thickness and domain size of the BaTiO_3 layers. The spontaneous polarization in the BaTiO_3 layers becomes zero at T_c , and the predicted T_c values agree with those from the Raman data. This is remarkable considering that no fitting parameters from the Raman experiments are used in the calculations.

In Fig. 4, T_c determined by the Raman data, x-ray diffraction (XRD), and the phase-field model are shown as a function of the BaTiO_3 and SrTiO_3 layer thicknesses. The XRD measurement provides an additional confirmation of the Raman results, where a change in the temperature dependence of the out-of-plane lattice constant can be taken as an indication of T_c (12). The figure shows that the BaTiO_3 layers in the superlattices are ferroelectric even when their thickness is only one unit cell, with a T_c as high as 250 K. T_c increases with increasing n as the dipole-dipole interaction in BaTiO_3 layers becomes stronger, whereas large m suppresses T_c by reducing the coupling between the BaTiO_3 layers. By changing the values of n and m , we were able to tune T_c from 151 to 638 K; that is, from 250 K below to 235 K above the bulk value of BaTiO_3 . The higher-than-bulk T_c is due to the strain in the BaTiO_3 layers, just as strain enhances T_c in single-layer ferroelectric films (26, 27). When the strain is partially relaxed in sample $(\text{BTO}_8/\text{STO}_4) \times 40$, T_c drops almost to the bulk BaTiO_3 value. Although the 3D phase-field model allowing domain formation provides a good description of the Raman data, simulations assuming a single domain in the BaTiO_3 layers yield significantly lower T_c for $m = 13$, demonstrating the importance of domain formation in theoretical calculations (28).

We now can conclude that ferroelectricity can be very strong in one-unit-cell-thick BaTiO_3 layers ($T_c \sim 250$ K for $n/m = 1/4$). The electrical boundary condition plays a critical role. With the highly polarizable SrTiO_3 in contact with the BaTiO_3 layers, the critical thickness is reduced to a single unit cell. Meanwhile, the mechanical boundary condition imposed by the SrTiO_3 substrate leads to strain in the BaTiO_3 layers and thus to enhanced ferroelectricity. The in-

terplay between the electrical and mechanical boundary conditions enables the tuning of T_c by nearly 500 K.

References and Notes

- C. H. Ahn, K. M. Rabe, J.-M. Triscone, *Science* **303**, 488 (2004).
- J. Junquera, P. Ghosez, *Nature* **422**, 506 (2003).
- D. D. Fong *et al.*, *Science* **304**, 1650 (2004).
- T. Tybell, C. H. Ahn, J.-M. Triscone, *Appl. Phys. Lett.* **75**, 856 (1999).
- H. N. Lee, H. M. Christen, M. F. Chisholm, C. M. Rouleau, D. H. Lowndes, *Nature* **433**, 395 (2005).
- M. E. Lines, A. M. Glass, *Principles and Applications of Ferroelectrics and Related Materials* (Clarendon, Oxford, 1977).
- A. A. Sirenko *et al.*, *Nature* **404**, 373 (2000).
- T. Ostapchuk *et al.*, *Phys. Rev. B* **66**, 235406 (2002).
- R. S. Katiyar, Y. I. Yuzuyk, R. R. Das, P. Bhattacharya, V. Gupta, *Ferroelectrics* **329**, 907 (2005).
- K. van Benthem, C. Elsässer, R. H. French, *J. Appl. Phys.* **90**, 6156 (2001).
- L. H. Tisinger *et al.*, *J. Vac. Sci. Technol. B* **21**, 53 (2003).
- See supporting material on Science Online for details.
- D. G. Schlom *et al.*, *Mater. Sci. Eng. B* **87**, 282 (2001).
- A. Scalabrin, A. S. Chaves, D. S. Shim, S. P. S. Porto, *Phys. Status Solidi B* **79**, 731 (1977).
- D. A. Tenne *et al.*, *Phys. Rev. B* **69**, 174101 (2004).
- P. A. Fleury, J. M. Worlock, *Phys. Rev.* **174**, 613 (1968).
- W. G. Nilsen, J. G. Skinner, *J. Chem. Phys.* **48**, 2240 (1968).
- B. Jusserand, M. Cardona, *Light Scattering in Solids V* (Springer, Heidelberg, Germany, 1989), pp. 49–152.
- C. Colvard *et al.*, *Phys. Rev. B* **31**, 2080 (1985).
- M. Trigo, A. Bruchhausen, A. Fainstein, B. Jusserand, V. Thierry-Mieg, *Phys. Rev. Lett.* **89**, 227402 (2002).
- A. Bartels, T. Dekorsy, H. Kurz, K. Köhler, *Phys. Rev. Lett.* **82**, 1044 (1999).
- L. E. Cross, in *Ferroelectric Ceramics*, N. Setter, E. L. Colla, Eds. (Birkhäuser Verlag, Basel, Switzerland, 1993), pp. 1–85.
- K. A. Müller, H. Burkard, *Phys. Rev. B* **19**, 3593 (1979).
- L.-Q. Chen, *Annu. Rev. Mater. Res.* **32**, 113 (2002).
- L.-Q. Chen, J. Shen, *Comput. Phys. Commun.* **108**, 147 (1998).
- K. J. Choi *et al.*, *Science* **306**, 1005 (2004).
- J. H. Haeni *et al.*, *Nature* **430**, 758 (2004).
- V. A. Stephanovich, I. A. Luk'yanchuk, M. G. Karkut, *Phys. Rev. Lett.* **94**, 047601 (2005).
- We thank L. Bergman for her help in the early stage of this work. This work was partially supported by the U.S. Department of Energy (DOE) under grant no. DE-FG02-01ER45907 (X.X.X.); by the Office of Naval Research under grant nos. N00014-03-1-0721 (D.G.S.), N00014-04-1-0426 (D.G.S.), N00014-03-1-0534 P0005 (A.F.), N00014-05-1-0559 (C.B.E.), N00014-00-1-0261 (K.M.R.), and N00014-01-1-0365 (K.M.R.); by NASA under grant no. NASA3-NCC1034 (R.S.K.); by NSF under grant nos. DMR-0507146 (D.G.S., L.Q.C., X.Q.P., K.M.R., and X.X.X.), DMR-0122638 (L.Q.C.), DMR-0213623 (L.Q.C.), DMR-0313764 (C.B.E.), ECS-0210449 (C.B.E.), and DMR-0315633 (X.Q.P.); and by a Guggenheim fellowship (L.Q.C.). The work at Los Alamos National Laboratory was supported by the Laboratory-Directed Research and Development Program under DOE.

Supporting Online Material

www.sciencemag.org/cgi/content/full/313/5793/1614/DC1
Materials and Methods
Figs. S1 to S6
References

22 May 2006; accepted 31 July 2006
10.1126/science.1130306